Constraint analysis of Curved Wide Plate Specimens

Matthias Verstraete[1,a], Wim De Waele[1,b], Stijn Hertelé[1,c],

Koen Van Minnebruggen[1,d] and Rudi Denys[1,e]

[1]Ghent University, Department of Mechanical Construction and Production, Laboratory Soete,
Technologiepark 903, 9052 Zwijnaarde, Belgium

[a]Matthias.Verstraete@UGent.be, [b]Wim.DeWaele@UGent.be, [c]Stijn.Hertele@UGent.be,

[d]Koen.VanMinnebruggen@UGent.be, [e]Rudi.Denys@UGent.be

Abstract Curved Wide Plate (CWP) testing has since long been applied to assess the integrity of defected girth welds. CWP specimens with (artificial) girth weld defect are loaded in tension and thus not subjected to a biaxial loading as is the case for pressurized pipes. This paper aims to evaluate the constraint ahead of the crack tip in pipe and CWP specimens. Therefore, crack tip stress fields obtained from finite element simulations have been analyzed using the two-parameter *JQ* framework. First, a comparison has been made between pressurized and unpressurized pipes. No pronounced influence of the pressure has been identified. Second, the CWP specimens have been compared to unpressurized pipe specimens. It is concluded that the CWP specimens are slightly conservative; they show a slightly higher constraint ahead of the crack tip. This conservatism increases with increasing defect dimensions.

Introduction

The construction of a transportation pipeline requires connecting different pipe sections by means of girth welds. To assess the severity of possible weld defects, the loading conditions should be estimated. Severe loading arises when a pipeline experiences large (plastic) deformation during operation, e.g. due to landslides [1]. The combination of internal pressure and axial deformation creates a biaxial loading condition.

To assess the criticality of girth weld defects, Curved Wide Plate (CWP) specimens have since long been used. A CWP specimen is a large panel extracted from a pipe, with an artificially notched girth weld at the mid-section. These specimens are tensile loaded up to the event of failure (fracture, pop-through, section yielding). Next to the obvious difference in pipe and CWP specimen geometry, a significant difference in the loading condition (presence of internal pressure) exists. Therefore, it might be questioned whether the constraint in CWP specimens represents that in pressurized pipes. Within the framework of this paper, the focus is on homogeneous, non-welded, specimens. Future research will also take mismatch effects in account.

To assess the constraint conditions, this paper evaluates the crack tip stress fields through detailed finite element simulations. First, a comparison is made between pipe tension tests with and without internal pressure to investigate the influence of biaxial loading. Next, the constraint level in CWP specimens is compared to the full pipe behavior.

Method

Finite element models have been created representing different specimen geometries and varying material properties. This paragraph first describes the analysis approach. Next, the finite element models are outlined, followed by an overview of the test matrix.

Constraint Analysis. For the analysis of the crack tip stress fields, the *JQ*-theory developed by Shih and O'Dowd [2, 3] has been applied. This two-parameter fracture mechanics framework aims at describing both the shape and magnitude of the crack tip stress fields. Within this framework, the *Q*-parameter describes a uniform hydrostatic shift between the actual crack tip opening stress, $\sigma_{\vartheta\vartheta}$, and the crack tip opening stress obtained from a reference field, $(\sigma_{\vartheta\vartheta})_{ref}$.

$$Q = \frac{\sigma_{\vartheta\vartheta} - (\sigma_{\vartheta\vartheta})_{ref}}{\sigma_{yield}} \tag{1}$$

Originally the Hutchinson-Rice-Rosengren field [4] was taken for the reference field was. However, nowadays the Small Scale Yielding (SSY) solution is frequently considered. This SSY solution is obtained from a Modified Boundary Layer (MBL) analysis, which represents high constraint plane strain conditions [5, 6]. The *Q*-parameter, as defined in Eq.1, is determined at a normalized distance, $r = 2J/\sigma_{yield}$, ahead of the crack tip.

Furthermore, it is to be noted that the *Q*-parameter is evaluated in the plane of the semi-elliptical crack ($\vartheta = 0$) at the deepest point of the crack. This point is known to have the highest crack driving force for long and shallow defects and is therefore believed to govern fracture.

Finite Element Models. A set of finite element models for Abaqus® 6.11 has been created through Python scripting as explained in [7]. These parametric scripts allow a well structured analysis of different material properties, geometries and loading conditions. In addition, this scripting approach assures a consistent and structured mesh design in the vicinity of the crack tip, suitable for analysis at high plastic deformation levels.

All models are characterized by an initial root radius (r_0) of 75 μm, a pipe outer diameter (*OD*) of 762 mm (30") and a wall thickness (*t*) of 15 mm. The steady crack has a semi-elliptical shape characterized by the crack depth (*a*) and crack length (*2c*). The pipe specimens have a length to diameter ratio equal to four, sufficient to avoid boundary effects at the crack [8]. The geometry of the CWP specimens is in agreement with the UGent guidelines for CWP testing [9]; the specimens have a prismatic section of 300 mm by 900 mm. For the determination of the reference stress field, a modified boundary layer model has been used. The reader is referred to [10] for details regarding this model.

Within the current set of finite element analyses, specimens with homogeneous Ramberg-Osgood material properties have been considered.

$$\varepsilon = \frac{\sigma}{E} + 0.002 \left(\frac{\sigma}{\sigma_{yield}} \right)^n \tag{2}$$

A fixed Young's modulus, *E*, of 206980 MPa and Poison coefficient, *v*, of 0.3 have been taken. The yield strength of the material has been fixed at 420 MPa. Furthermore, ε represents the true strain, σ the true stress and *n* the strain hardening exponent in the above equation.

A mesh convergence study indicated mesh-independent results for *J*-integral calculations using approximately 45000 linear brick elements with a reduced integration scheme (Abaqus® type C3D8R) for pipe specimens (see Figure 1a) and 25000 elements for CWP specimens (see Figure 1b). In the vicinity of the crack tip, a gradually coarsening spider web mesh has been applied (see Figure 1c).
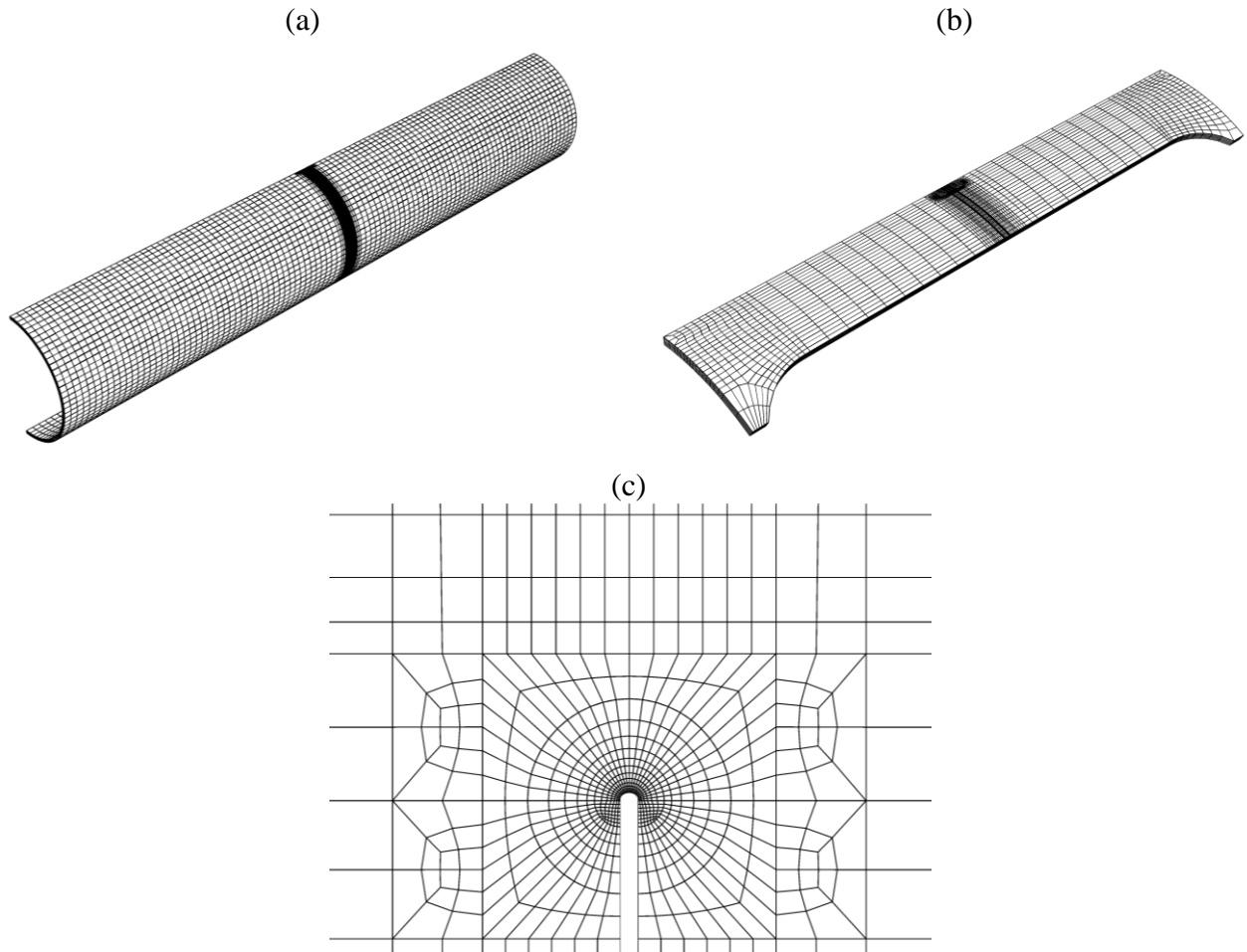
(a)   (b)

(c)

Figure 1. Overview of mesh in pipe specimen (a), CWP specimen (b) and detail
of mesh around initially blunted crack tip (c)

Aiming to approximate the actual loading conditions, displacement boundary conditions are applied at the free ends of the pipe and curved wide plate specimens. In addition, symmetry boundary conditions allow modeling only half the specimens. In case of internal pressure, a constant pressure is applied on the inner diameter of the pipe. For inner diameter defects, pressure is also applied on the crack faces. The magnitude of the pressure is characterized by its resulting hoop stress, σ_{hoop}.

Test Matrix. An overview of all discussed simulations is given in Table 1. First, the influence of internal pressure has been considered by comparing both pressurized and unpressurized pipes. Second, a comparison between unpressurized pipes and CWP specimens has been performed. Crack sizes and strain hardening coefficients, *n*, have been varied.

Table 1. Overview of performed simulations

Parameter set	a/t [-]	$2c$ [mm]	$\sigma_{hoop}/\sigma_{yield}$ [-]	n [-]	Defect location	Geometry
S_0	0.2	25	0	10	ID	Pipe, CWP
S_1	0.2	25	0	10	*OD*	Pipe, CWP
S_2	0.2	25	*0.1*	10	ID	Pipe
S_3	0.2	25	*0.3*	10	ID	Pipe
S_4	0.2	25	*0.5*	10	ID	Pipe
S_5	0.2	25	*0.8*	10	ID	Pipe
S_6	0.2	25	*1.0*	10	ID	Pipe
S_7	0.2	25	*0.8*	10	*OD*	Pipe
S_8	*0.4*	25	0	10	ID	Pipe, CWP
S_9	0.2	*50*	0	10	ID	Pipe, CWP
S_{10}	0.2	*100*	0	10	ID	Pipe, CWP
S_{11}	0.2	25	0	*15*	ID	Pipe, CWP
S_{12}	0.2	25	0	*20*	ID	Pipe, CWP

Results and Discussion

Influence of Crack Tip Radius. In practice the crack tip radius of a crack is often assumed to be infinitely sharp. However, since the developed models aim to represent fully plastic conditions, modeling of an initially blunted crack is advised [11]. To evaluate the influence of this initial blunting, MBL analyses have been performed with a crack tip radius equal to 75.0 µm, the boundary conditions representing an equivalent load level of $J = 2500$ N/mm. Subsequently, the crack tip stress fields have been plotted for increasing load levels. Illustrated in Figure 2 is the convergence of the crack tip stress fields at higher load levels. The influence of the initial blunting fades out.
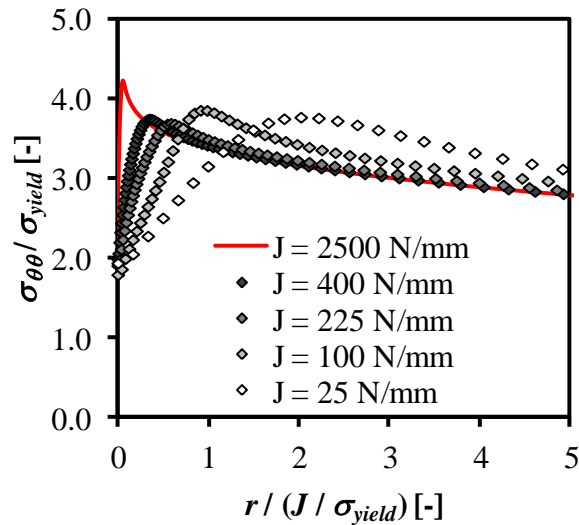

Figure 2. Influence of equivalent J load level in MBL with initially blunted crack ($r_0 = 75$ µm)

As the *JQ*-trajectories are calculated at a normalized distance ahead of the crack tip $r/(J/\sigma_{yield}) = 2$, the influence of the initial blunting is evaluated based on the stress amplitude at this location. In order to limit the error of the normalized stress to 1%, a crack tip opening displacement of three times the initial crack tip radius is required (see Figure 3).

For the *JQ*-calculations, the reference field from the MBL model is obtained at an equivalent load level of $J = 2500$ N/mm. However, anomalous *Q*-values are expected at low load levels in pipe and CWP specimens, since these also have an initially blunted crack. The theoretical relation between crack tip opening displacement (CTOD) and J-integral is given by:

$$CTOD = m \frac{J}{\sigma_{yield}}$$ (3)

Based on finite element simulations, a conversion factor, *m*, of 0.59 is identified for pipe specimens. Accordingly, a realistic lower level for valid *JQ*-pairs corresponds with a *J*-value of 160 N/mm. Indeed, the trend in the *JQ*-curves becomes obvious from this load level, illustrated in Figure 4. Accordingly, the *JQ*-trajectories plotted in the remainder of this paper will only show results for *J*-values beyond 160 N/mm.
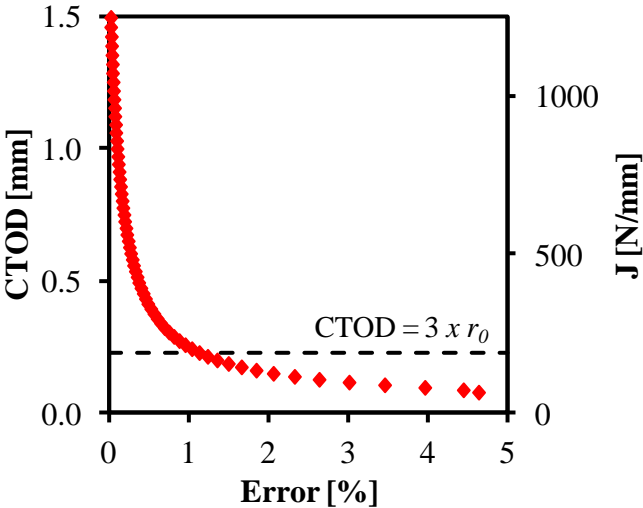

Figure 3. Relative error of crack tip stress field at normalized distance ahead of crack tip equal to $r/(J/\sigma_{yield}) = 2$ for initially blunted crack with radius $r_0 = 75$ µm.
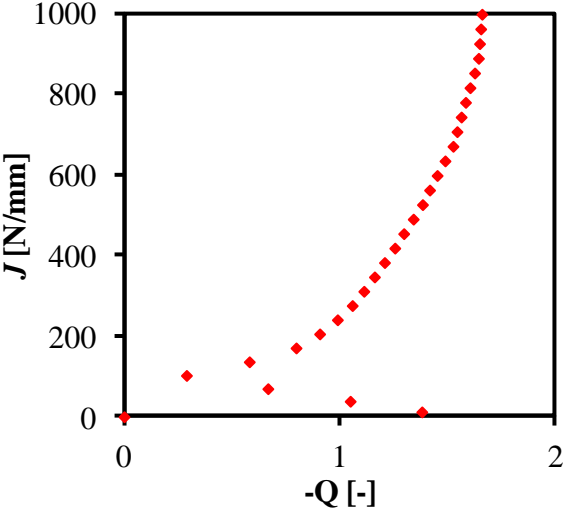

Figure 4. *JQ*-trajectory for pressurized pipe indicating some anomalous *JQ*-pairs at low load levels (Parameter set S_0)

Influence of internal pressure. To evaluate the influence of the internal pressure on the constraint level ahead of the crack tip, simulations have been performed on pipes with several levels of internal pressure. Expressed in terms of the resulting hoop stress relative to the yield strength of the material, internal pressure levels ranging from 0% to 100% have been examined. First, a loss of constraint is observed upon the development of plasticity; larger *J*-values correspond to lower *Q*-values. Second, it is observed that the internal pressure only marginally shifts the constraint ahead of the crack tip, see Figure 5a. A more detailed view, e.g. for load level *J* = 400N/mm as shown in Figure 5b, reveals that the *Q*-parameter marginally increases at low pressure levels, remaining close to constant for higher relative pressure levels.
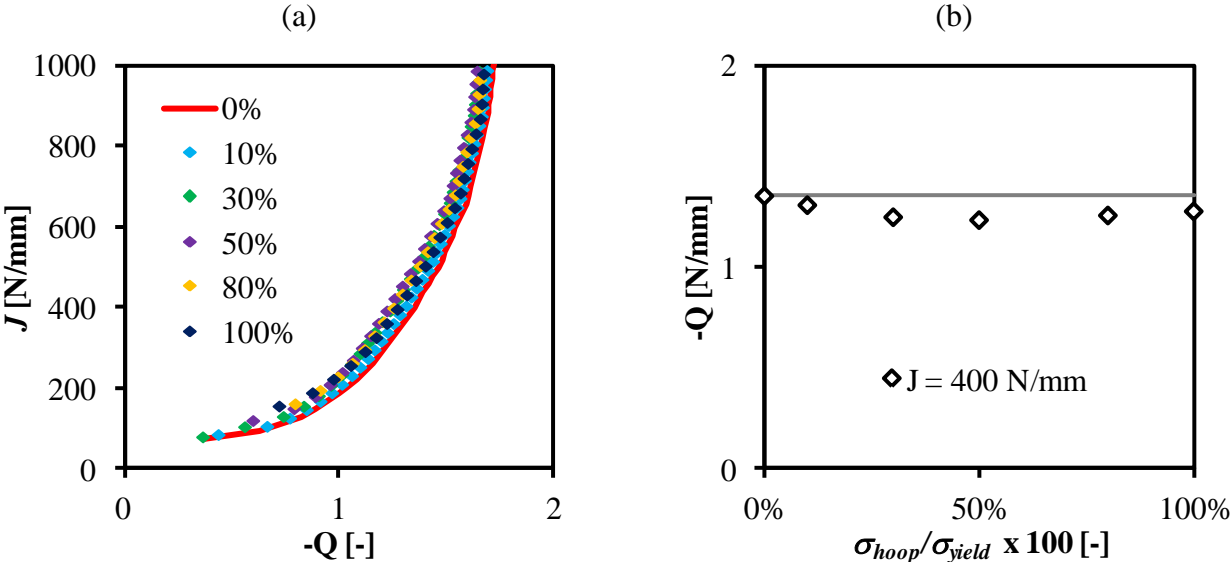

(a)   (b)

Figure 5. Influence of internal pressure on *JQ*-trajectories for internal diameter defects with varying levels of $\sigma_{hoop}/\sigma_{yield}$ (Parameter set S$_0$, S$_{2\text{-}6}$)

The above comparison relates to inner diameter defects, thus subjected to internal pressure acting on the crack faces. Next, a similar study has been performed for outer diameter defects. Shown in Figure 6 are the *JQ*-trajectories for both pressurized and unpressurized pipes with inner and outer diameter defects. A marginal difference is observed between both curves, indicating that the absence of the pressure on the crack faces does not significantly affect the constraint.

From the above observations it is concluded that internal pressure does not significantly shift the constraint level ahead of the crack tip at the deepest point of the crack. This observation is in agreement with published results of Cravero et al. [12].
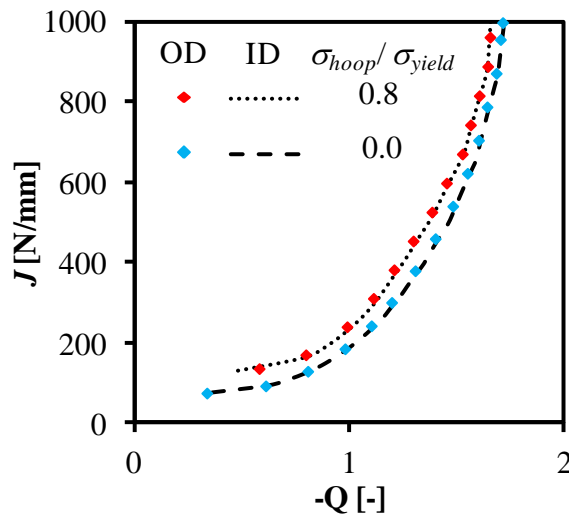
Figure 6. Influence of internal pressure in case of outer and inner diameter defect
(Parameter set S_0 vs. S_1 and S_5 vs. S_7)

Constraint in CWP specimens. An set of CWP specimens with varying material properties and defect dimensions has been analyzed. At first, the *JQ*-trajectories have been compared for varying crack sizes, shown in Figure 7. In general the *JQ*-trajectories of the CWP specimens are slightly higher than those of the unpressurized pipe specimens, although for higher load levels both converge. Consequently, the CWP test can be seen as a conservative representation of the full scale behavior in terms of crack tip constraint.
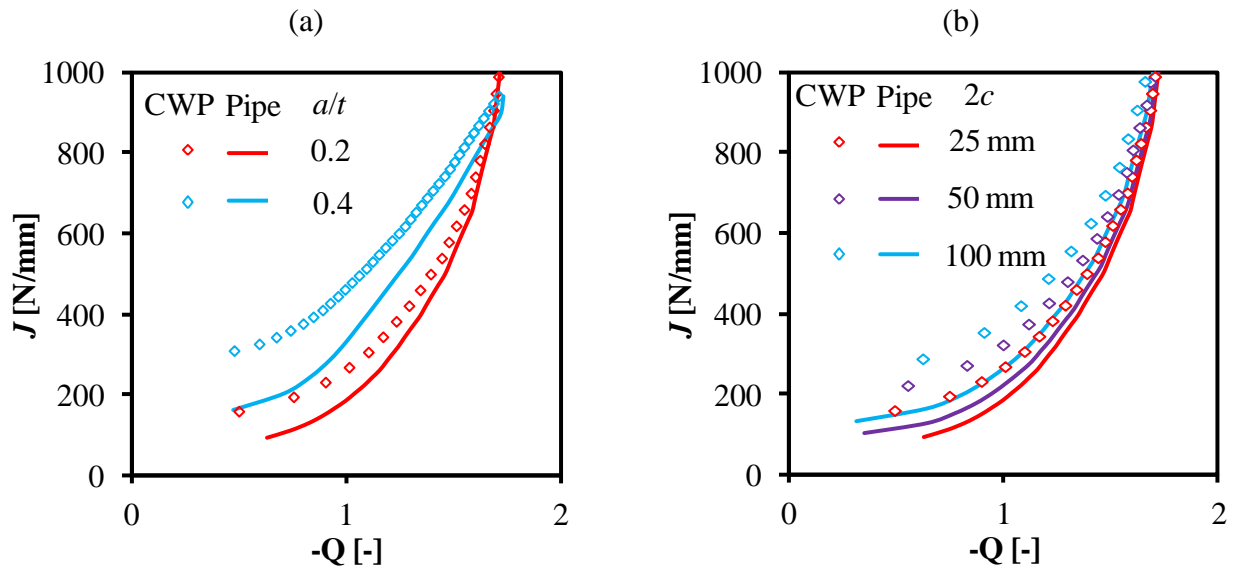
(a)   (b)

Figure 7. Influence of relative crack depth (a) and length (b) on constraint in CWP and unpressurized pipe specimens

Focusing on the relative crack depths, it is observed that for higher *a/t*-values the constraint ahead of the crack tip increases, represented by higher *Q*-values. This trend is observed for both CWP and unpressurized pipe specimens. The higher constraint for higher relative crack depths is assumed to be caused by an increased bending of the cracked ligament. In addition, this bending influences the difference between the CWP and pipe specimen. For the CWP specimens no axial symmetry

constrains bending at the cracked ligament, as is the case for the pipe specimens. Consequently, it is well understood that the constraint-related conservatism involved in CWP testing increases for higher crack sizes.

Second, the influence of the material properties is evaluated. Within the framework of this paper, the focus is on the influence of the strain hardening exponent. Analyses of three different strain hardening exponents indicate that a truly limited difference occurs, see Figure 8. This indicates that the constraint in curved wide plate and pipe specimens is related to the geometry rather than the material properties.
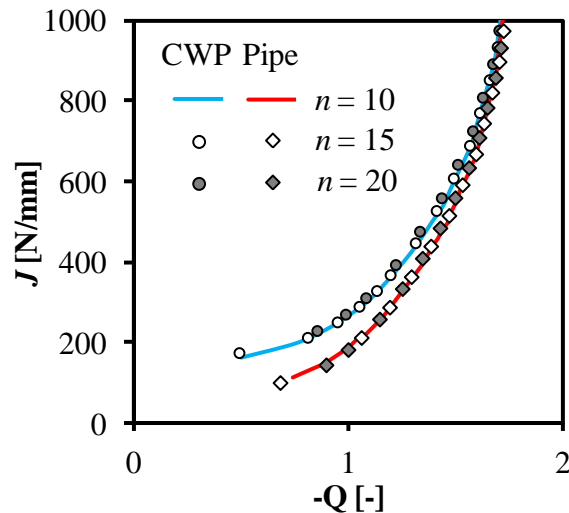

Figure 8. Influence of strain hardening properties on JQ-trajectories for CWP and unpressurized pipe specimens

Conclusion
A comparison has been made between the crack tip stress fields of pressurized and unpressurized pipes as well as Curved Wide Plate specimens. From this comparison it is concluded that:
- If an initially blunted crack tip is modeled, the analysis of the crack tip stress fields is influenced by this initial blunting for load levels up to a crack tip opening displacement (CTOD) of three times the initial crack tip radius.
- The internal pressure does not significantly shift the constraint ahead of the crack tip in pipe specimens.
- The constraint in Curved Wide Plate specimens is slightly higher than in pipe specimens. This conservatism increases with crack size.

References

1.	Lillig, D.B., *The first (2007) ISOPE strain-based design symposium - a review*, in *International offshore and polar engineering conference*. 2008: Vancouver, BC, Canada.
2.	O'Dowd, N.P. and Shih, C.F., *Family of crack-tip fields characterized by triaxiality parameter: Part I - structure of fields.* Journal of Mechanics and Physics of Solids, 1991. **39**(8): p. 989-1015.
3.	O'Dowd, N.P. and Shih, C.F., *Family of crack-tip fields characterized by triaxiality parameter: Part II - application.* Journal of Mechanics and Physics of Solids, 1992. **40**(5): p. 939-963.
4.	Anderson, T.L., *Fracture mechanics: fundamentals and applications*. 2nd ed. 1995: C. Press.
5.	Dodds, R.H., Shih, C.F. and Anderson, T.L., *Continuum and micromechanics treatment of constraint in fracture*. 1993, Office of nuclear regulatory research.
6.	O'Dowd, N.P., *Applications of two parameter approaches in elastic-plastic fracture mechanics.* Engineering Fracture Mechanics, 1995. **52**(3): p. 445-465.
7.	Hertele, S., De Waele, W. and Denys, R., *A generic stress-strain model for metallic materials with two-stage strain hardening behaviour.* International Journal of Non-Linear Mechanics. **46**(3): p. 519-531.
8.	Kibey, S.A., Lele, S.P., Tang, H., Macia, M.L., Fairchild, D.P., Cheng, W., Noecker, R., Wajutelewicz, P.J., Newbury, B., Kan, W.C. and Cook, M.F., *Full-scale test observations for measurement of tensile strain capacity of welded pipelines*, in *International Offshore and Polar Engineering Conference*. 2011: Maui, Hawaii, USA.
9.	Denys, R. and Lefevre, T.L., *UGent guidelines for Curved Wide Plate testing*, in *Pipeline Technology Conference*. 2009: Ostend, Belgium.
10.	Verstraete, M., De Waele, W. and Hertelé, S., *Development and validation of a high constraint modified boundary layer finite element model*, in *Sustainable construction and design*. 2011: Gent, Belgium.
11.	*ABAQUS 6.11 Analysis User's Manual: Constructing a fracture mechanics mesh for finite-strain analysis with the conventional finite element method*.
12.	Cravero, S., Bravo, R.E. and Ernst, H.A., *Fracture evaluation of cracked pipelines subjected to combined loading*, in *Pipeline Technology Conference*. 2009: Ostend, Belgium.